Contents (this .pdf):

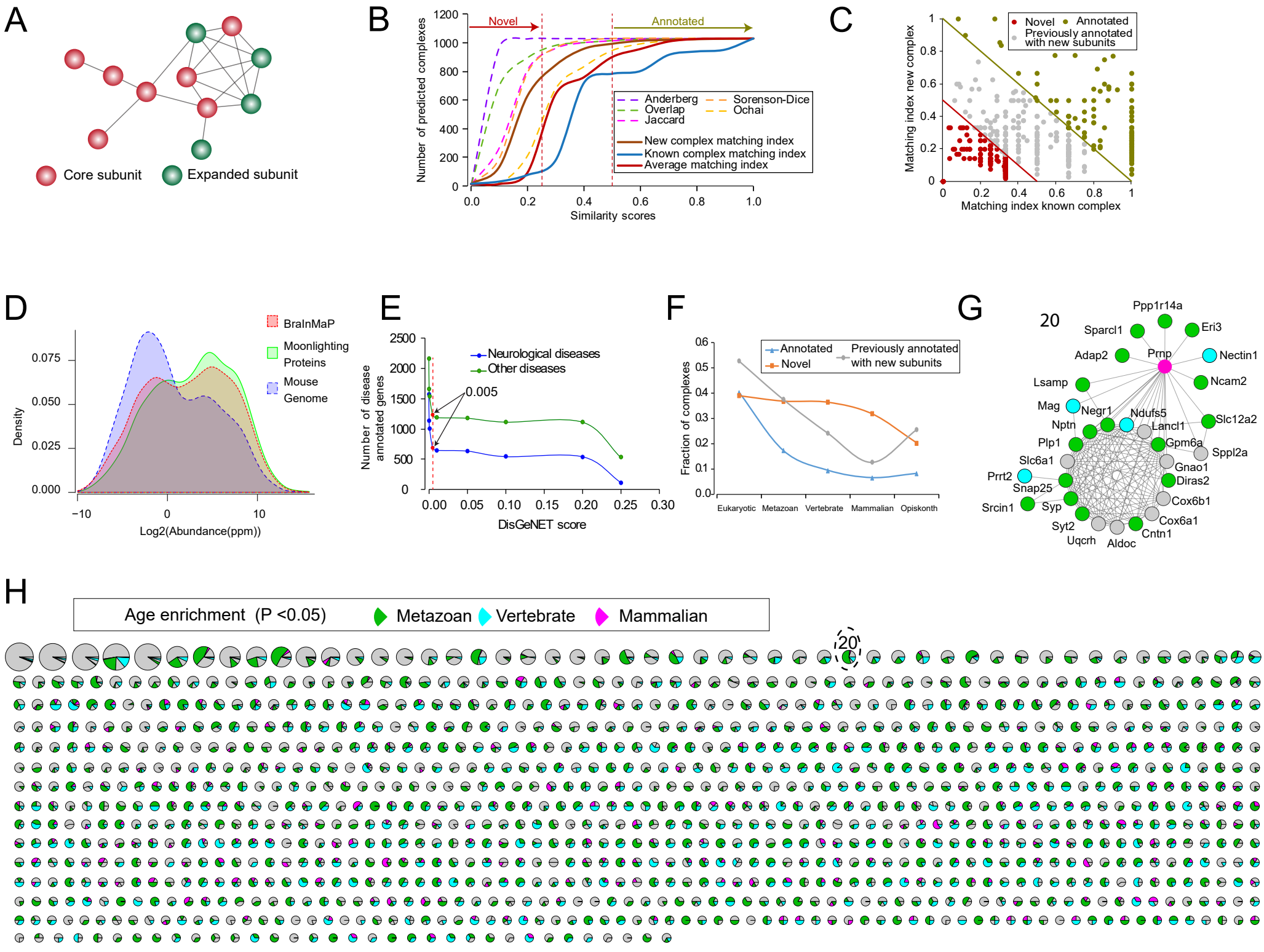
A
Core subunit
Expanded subunit
B
Novel
Annotated
Number of predicted complexes
Similarity scores
Anderberg
Overlap
Jaccard
Sorenson-Dice
Ochai
New complex matching index
Known complex matching index
Average matching index
C
Novel
Annotated
Previously annotated with new subunits
Matching index new complex
Matching index known complex
D
BraInMaP
Moonlighting Proteins
Mouse Genome
Density
Log2(Abundance(ppm))
E
Neurological diseases
Other diseases
0.005
Number of disease annotated genes
DisGeNET score
F
Annotated
Novel
Previously annotated with new subunits
Fraction of complexes
Eukaryotic
Metazoan
Vertebrate
Mammalian
Opiskonth
G
20
Ppp1r14a
Sparcl1
Eri3
Adap2
Prnp
Nectin1
Lsamp
Ncam2
Mag
Negr1
Ndufs5
Slc12a2
Nptn
Lancl1
Plp1
Gpm6a
Sppl2a
Slc6a1
Gnao1
Prrt2
Diras2
Snap25
Cox6b1
Srcin1
Syp
Cox6a1
Syt2
Cntn1
Uqcrh
Aldoc
H
Age enrichment (P <0.05)
Metazoan
Vertebrate
Mammalian
20

FIGURE S1

A Deconstructed complex ‘core’ and ‘expanded’ components of the merged network.

B Distribution of six different similarity metrics used to establish the novelty of predicted assemblies.

C Scatterplot of average matching index for annotated, substantively annotated and novel complexes.

D Density distribution plot comparing the abundance of moonlighting proteins (subunits belonging to multiple complexes) in BraInMap, or the mouse genome.

E Distribution of disease associated genes in BraInMap complexes.

F Age distribution of BraInMap complexes.

G Exemplar Complex 20 showing the age of each subunit.

H Conservation and age of brain protein complexes, as determined by ortholog prediction (see STAR methods), colored according to the frequency of proteins in assigned ‘age’ categories according to phylogenetic origin: Eukaryotic (*grey*), Metazoan (*green*), Vertebrate (*blue*) or Mammalian (*cyan*).

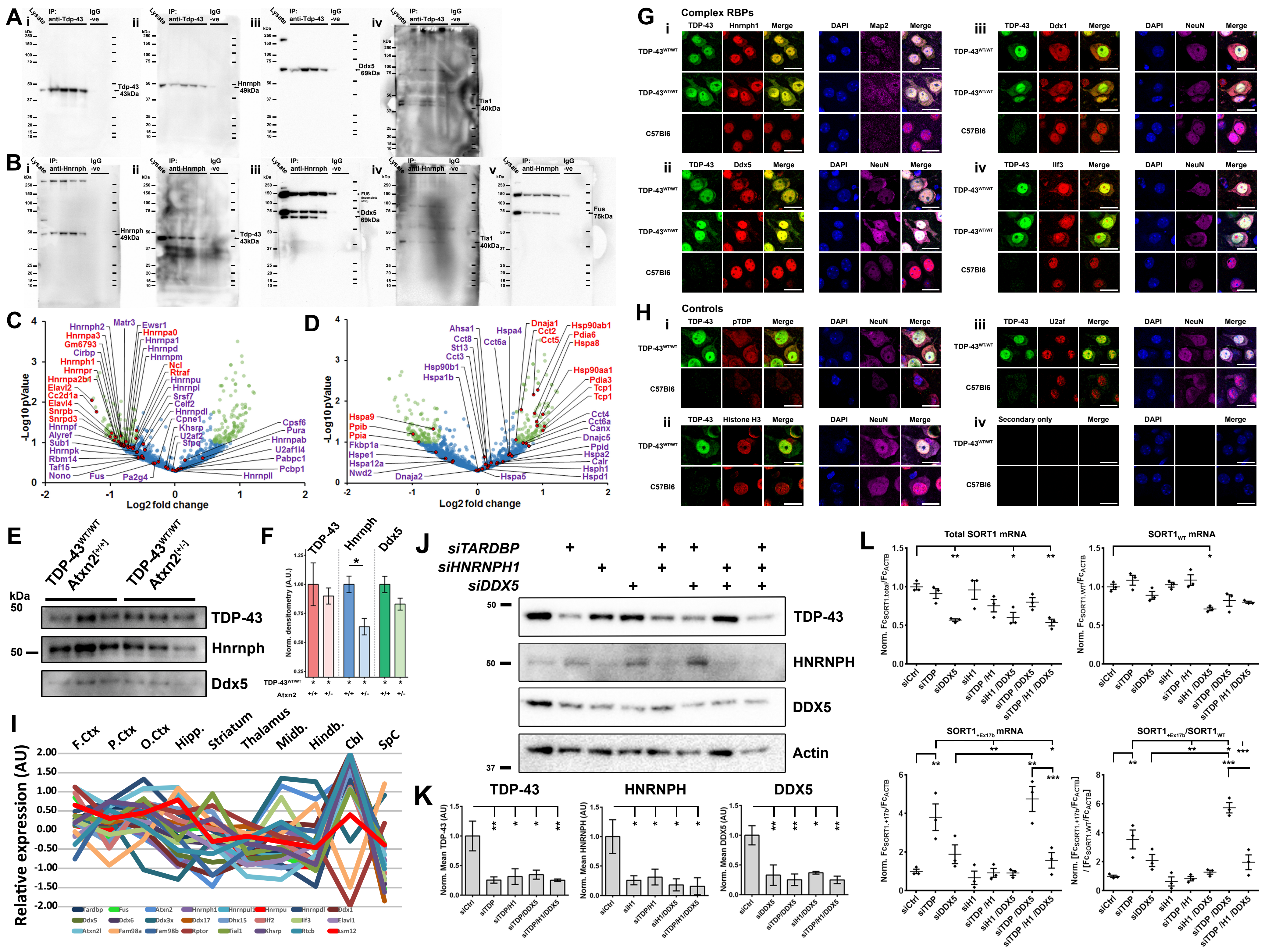
A
Lysate
IP: anti-Tdp-43
IgG -ve
Tdp-43 43kDa
Hnrnph 49kDa
Ddx5 69kDa
Tia1 40kDa
B
IP: anti-Hnrnph
Hnrnph 49kDa
Tdp-43 43kDa
FUS
Ddx5 69kDa
Tia1 40kDa
Fus 75kDa
C
-Log10 pValue
Log2 fold change
Hnrnph2
Matr3
Ewsr1
Hnrnpa3
Hnrnpa0
Gm6793
Hnrnpa1
Hnrnpd
Cirbp
Hnrnpm
Hnrnph1
Ncl
Hnrnpr
Rtraf
Hnrnpa2b1
Hnrnpu
Elavl2
Hnrnpl
Cc2d1a
Srsf7
Elavl4
Celf2
Snrpb
Hnrnpdl
Snrpd3
Cpne1
Hnrnpf
Khsrp
Alyref
U2af2
Sub1
Sfpq
Hnrnpk
Rbm14
Taf15
Nono
Fus
Pa2g4
Cpsf6
Pura
Hnrnpab
U2af1l4
Pabpc1
Pcbp1
Hnrnpll
D
Ahsa1
Hspa4
Dnaja1
Hsp90ab1
Cct2
Pdia6
Cct8
Cct6a
Cct5
Hspa8
St13
Cct3
Hsp90b1
Hsp90aa1
Hspa1b
Pdia3
Tcp1
Tcp1
Hspa9
Cct4
Ppib
Cct6a
Ppia
Canx
Fkbp1a
Dnajc5
Hspe1
Ppid
Hspa12a
Hspa2
Nwd2
Calr
Dnaja2
Hspa5
Hsph1
Hspd1
E
TDP-43WT/WT Atxn2[+/+]
TDP-43WT/WT Atxn2[+/-]
kDa
TDP-43
Hnrnph
Ddx5
F
TDP-43
Hnrnph
Ddx5
Norm. densitometry (A.U.)
TDP-43WT/WT
Atxn2
+/+
+/-
G
Complex RBPs
TDP-43
Hnrnph1
Merge
DAPI
Map2
NeuN
Ddx1
Ddx5
Ilf3
TDP-43WT/WT
C57Bl6
H
Controls
pTDP
Histone H3
U2af
Secondary only
I
F.Ctx
P.Ctx
O.Ctx
Hipp.
Striatum
Thalamus
Midb.
Hindb.
Cbl
SpC
Relative expression (AU)
Tardbp
Fus
Atxn2
Hnrnph1
Hnrnpul1
Hnrnpu
Hnrnpdl
Ddx1
Ddx5
Ddx6
Ddx3x
Ddx17
Dhx15
Ilf2
Ilf3
Elavl1
Atxn2l
Fam98a
Fam98b
Rptor
Tial1
Khsrp
Rtcb
Lsm12
J
siTARDBP
siHNRNPH1
siDDX5
TDP-43
HNRNPH
DDX5
Actin
K
TDP-43
HNRNPH
DDX5
Norm. Mean TDP-43 (AU)
Norm. Mean HNRNPH (AU)
Norm. Mean DDX5 (AU)
siCtrl
siTDP
siTDP/H1
siTDP/DDX5
siTDP/H1/DDX5
siH1
siH1/DDX5
siDDX5
L
Total SORT1 mRNA
SORT1WT mRNA
SORT1+Ex17b mRNA
SORT1+Ex17b/SORT1WT
siCtrl
siTDP
siDDX5
siH1
siTDP /H1
siH1 /DDX5
siTDP /DDX5
siTDP /H1 /DDX5

FIGURE S2

A Immunoblots from immunoprecipitation of endogenous mouse Tdp-43. Relating to Figure 5D**.** Endogenous Tdp-43 was immunoprecipitated from the cortices of four wild type C57Bl/6J mice (MAb FL4 mouse anti-murine-Tdp-43), immunoblotted and probed for: A) TDP-43 (Proteintech; 12892-1-AP), B) hnRNP-H (Bethyl Labs; A300-511A), C) DDX5 (Abcam; ab21696), D) TIA1 (Santa Cruz; sc-1751). From these panels, cropped images were used to produce Figure 5D.

B Immunoblots from immunoprecipitation of endogenous mouse Hnrnph1. Relating to Figure 5E. Endogenous Hnrnph1 was immunoprecipitated from the cortices of four wild type C57Bl/6J mice (Bethyl Labs A300-511A, rabbit anti-hnRNP-H), immunoblotted and probed for: A) hnRNP-H (Santa Cruz; sc-10042), B) Tdp-43 (FL4, gift from Ling Shuo-Chien), C) DDX5 (Abcam; ab21696), D) TIA1 (Santa Cruz; sc-1751), E) FUS/TLS (Proteintech; 11570-1-AP). In panel iii, * indicates bands from incomplete stripping of FUS antibodies. From these panels, cropped images were used to produce Figure 5E.

C In the protected TDP-43$^{WT/WT}$Atxn2$^{[+/-]}$ mice, TDP-43 showed decreased interaction with proteins associated with RNA binding functional terms, this is exemplified by the volcano plot distribution of heterogeneous nuclear ribonucleoproteins (HNRNPs, each of which is labelled).

D Interestingly, TDP-43 in the protected TDP-43$^{WT/WT}$Atxn2$^{[+/-]}$ mice showed increased interaction with proteins clustering to functional categories such as protein folding, ATP binding, and sodium/potassium ion homeostasis, this is exemplified by the volcano plot distribution of heat shock proteins and protein isomerases that form the unfolded protein response (each of which is labelled). For volcano plots, points plots Log_2 fold change against $–Log_{10}$ P value for each detected protein from TDP-IP of transgenic mice. A Log_2 fold change <0 indicates reduced interaction with TDP-43 in the protected TDP-43$^{WT/WT}$Atxn2$^{[+/-]}$ versus TDP-43$^{WT/WT}$Atxn2$^{[+/+]}$ mice. Green points indicate significant difference TDP-43$^{WT/WT}$Atxn2$^{[+/+]}$ versus TDP-43$^{WT/WT}$Atxn2$^{[+/-]}$ (Log_2 fold change > ±0.58 and $-Log_{10}$ P value >1.0). Red points are proteins of interest with red text for proteins showing significant difference and purple text for proteins showing no significant difference.

E Immunoblots of immunoprecipitated material from transgenic mice confirm the interaction of TDP-43 with Hnrnph1 and Ddx5.

F Densitometric analysis of RBP signal (from blot in panel B; normalized to TDP-43 signal) indicates that TDP-43 has 36% decreased interaction with Hnrnph1 (SEM ±0.07, *P = 0.02) and a trend toward 17% decreased interaction with Ddx5 (SEM ±0.05, P = 0.11) in the protected TDP-43$^{WT/WT}$Atxn2$^{[+/-]}$ mice versus the affected TDP-43$^{WT/WT}$ mice.

G In affected cortical neurons of transgenic TDP-43$^{WT/WT}$ mice, nuclear RBPs that form complexes with TDP-43 redistribute into cytoplasmic phospho-TDP-43 (pS409/410) inclusions. Relating to Figure 6C. The distribution of RNA binding proteins i) Hnrnph1, ii) Ddx5, iii) Ddx1, and iv) Ilf3, that are components of the BraInMap complex 22, were investigated in transgenic TDP-43$^{WT/WT}$ and wildtype C57Bl6 mice by confocal immunofluorescent imaging. The cytoplasmic distribution of the RBPs mirrored that of TDP-43; for instance, neurons showing focal accumulations of TDP-43 also showed colocalized accumulations of complex 22 RBPs. These RBPs are restricted to the nuclei of neurons and of non-neurons in wild type C57Bl6 mice. Neurons were immunolabelled either with the neuron specific markers Map2 or NeuN. Cell nuclei were counterstained with DAPI. Scale bar = 20µm.

H i) Cytoplasmic TDP-43 was phosphorylated at S409/410 using a phospho-specific antibody (a gift from Leonard Petrucelli). ii) The RNA binding protein U2af, which is not a component of RBP complex 11, does not redistribute out of neuronal nuclei in TDP-43$^{WT/WT}$*Atxn2*$^{[+/+]}$ mice, nor does the nuclear protein Histone H3 (iii). Secondary (donkey) anti-mouse-AF488, anti-rabbit-AF594 and anti-chicken-AF647 antibodies were found not to label the tissue indicating the specificity of the primary antibodies (iv).

I Regional protein expression of TDP-43 and associated components of ALS-relevant BraInMap complex 22. Protein expression was quantified in dissected brain regions by mass spectroscopy then normalized to whole brain expression. Individual protein components of the ALS-relevant RBP complex 22 are plotted against the brain region.

J Immunoblots from siRNA knock down in SH-SY5Y. Relating to Figure 6E, F. Cultured SH-SY5Y cells were transfected with siTDP-43, siHNRNPH1 and siDDX5 for 72hrs before harvesting and immunoblotting siTDP-43 elicited a 65.5% to 74.8% knockdown of TDP-43 protein, siHNRNPH1 elicited a 68.7% to 84.4% knockdown of HNRNPH1 protein, siDDX5 elicited a 63.1% to 75.1% knockdown of DDX5 protein. Furthermore, these siRNA knockdown experiments confirm the specificity of the anti-hnRNP-H (Bethyl Labs; A300-511A) and anti-DDX5 (Abcam; ab21696) used for immunoblotting in **Figure 5D, E** (and **Figure S2A, B**) and for immunolabelling in **Figure 6C** (and **Figure S2G**).

K Graphs show mean ± SEM protein band densitometry. (N= 3 per treatment group, ANOVA w/ Dunnett's multiple comparison test against siCtrl group, * P< 0.05, ** P< 0.01). For Fig 5G, RBPs were similarly knocked down in SH-SY5Y and RNA collected for splicing analysis.

L Total *SORT1* mRNA, *SORT1*$_{WT}$ mRNA and *SORT1*$_{+Ex17b}$ mRNA transcript was quantified, normalized to ACTB and to the mean of the siControl (siCtrl) treated group. The relative ratio of exon 17b inclusion

was calculated as *SORT1*$_{+Ex17b}$/*SORT1*$_{WT}$. Scatter plots show individual data points with bars at mean ± SEM (N= 3 per treatment group, ANOVA w/ Tukey's multiple comparison test between all groups, * P< 0.05, ** P< 0.01, *** P< 0.001).